1

Introduction

Seizo Morita

Abstract. Since the publication of *Noncontact Atomic Force Microscopy* in 2002, the noncontact atomic force microscope (NC-AFM), which can image even insulators with atomic resolution, has achieved remarkable progress. This second volume deals with the following outstanding results obtained with atomic resolution after the publication of the previous books: (1) *Force Spectroscopy and Force-Mapping with Atomic Resolution*, (2) *Tuning Fork/qPlus Sensor*, (3) *Atomic Manipulation*, (4) *Magnetic Exchange Force Microscopy*, (5) *Atomic and Molecular Imaging in Liquids*, (6) *New Technologies in Dynamic Force Microscopy*. These results and technologies are now varying the NC-AFM with imaging function on an atomic scale toward characterization and manipulation tools of individual atoms/molecules and nanostructures with atomic/subatomic resolution. Therefore, the NC-AFM is now becoming a crucial tool for nanoscience and nanotechnology.

1.1 Rapidly Developing High Performance AFM

In the previous book published in 2002 [1], we mentioned that the atomic force microscope (AFM) is a unique microscope based on a mechanical method with the following features:

- True atomic resolution
- Observation of insulators
- Three-dimensional (3D) measurements of atomic-forces (atomic force spectroscopy [AFS])
- Control of atomic forces
- Measurement of mechanical response
- Mechanical manipulation of individual atoms
- Atom-by-atom mechanical assembly

In fact, the previous book reported true atomic resolutions on various semiconductor surfaces [Si(111)7×7, Si(100)2×1, Si(111)-c(4×2), GaAs(110), InP(110), InAs(110), Si(111)$\sqrt{3} \times \sqrt{3}$-Ag, Si(100)2×1:H, Si(100)1×1:2H,

S. Morita et al. (eds.), *Noncontact Atomic Force Microscopy*,
NanoScience and Technology,
DOI: 10.1007/978-3-642-01495-6_1,

Si(111)$5\sqrt{3} \times 5\sqrt{3}$-Sb, Ge/Si(111)] and HOPG. Besides, it observed atomic structures even on various ionic crystals [NaCl(100), KCl(100), KBr(100), SrF_2(111), CaF_2(111), BaF_2(111), $KCl_{0.6}Br_{0.4}$, NaCl/Cu(111), $CaCO_3$] and various metal oxides [NiO(001), $\alpha-Al_2O_3$(0001), TiO_2(110), TiO_2(100), SnO_2(110), Al_2O_3/NiAl(110), CeO_2(111), (H, K)/TiO_2(110)1×1]. Further, it achieved molecular/submolecular resolution on various molecules {(RCOO-/TiO_2) [R=H, CH_3, $C(CH_3)_3$, C ≡ CH, CHF_2, CF_3], C_{60}, adenine/HOPG, thymine/HOPG, DNA/mica, octanethiol, hexadecanthiol, alkanethiol/Au(111), dimethylquinquethiophene (DN5T), VDF oligomer, poly (vinylidene fluoride) [PVDF]}. Thus the previous book fully proved the ability of NC-AFM on true atomic resolution and observation of insulators with atomic resolution.

To measure three-dimensional (3D) atomic-forces (atomic force spectroscopy [AFS]), the previous book introduced two methods. In one method, the site-dependence of the site-specific frequency shift curve at atomically specified sites (A, B, C) was measured as shown in Fig. 1.1a, while, on the other method, the tip–sample distance dependence of the NC-AFM image at different atomic spacing (a, b, c) was measured as shown in Fig. 1.1b. Thermal

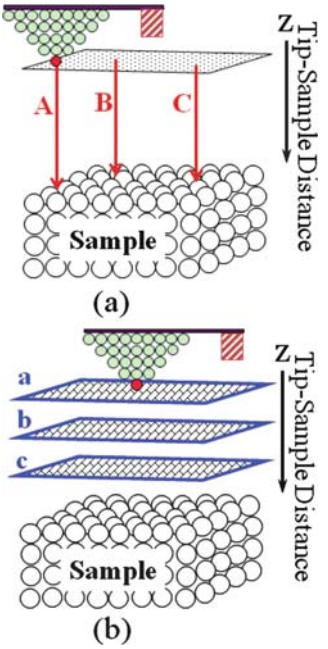

Fig. 1.1. Schematic model of atomic force spectroscopy to obtain a three-dimensional force-related map [1]. (**a**) The method using the site-dependent frequency-shift curves obtained at sites A, B, C, etc. (**b**) Alternating method using the tip–sample distance dependence of the NC-AFM images obtained at tip–sample distance a, b, c, etc.

drift along the sample surface at room temperature (RT), however, gradually shifted the tip apex outermost atom away from the atomically specified site and thus disturbed the former method that obtains the precise site-specific frequency shift curves at atomically specified sites. As a result, only at low temperature (LT) without thermal drift, the site-specific frequency shift curve measurements were achieved at atomically specified sites on a few limited samples such as Si(111)7×7 and graphite in 2002. Similarly, thermal drift perpendicular to the sample surface at RT gradually changed the atomic spacing and thus disturbed the latter method that obtains the tip–sample distance dependence of the NC-AFM image. As a result, atomically resolved NC-AFM images were acquired only at $2 \sim 3$ limited tip–sample distance in 2002. Now we can carry out precise force spectroscopy measurements and force-mapping with atomic resolution even at RT on various samples as introduced in this second volume.

To control atomic forces, measure mechanical response, and mechanically manipulate individual atoms, we have to precisely decrease and also control the tip–sample distance by varying the tip-to-sample gap from noncontact region toward nearcontact region as shown in Fig. 1.2. Precise control of tip–sample distance, however, was incomplete in 2002. As a result, control of atomic forces, measurement of mechanical response, and mechanical manipulation of individual atoms were tentatively investigated in 2002. Now we can precisely control tip–sample distance, and thus carry out precise control of atomic forces, measurement of mechanical response, and mechani-

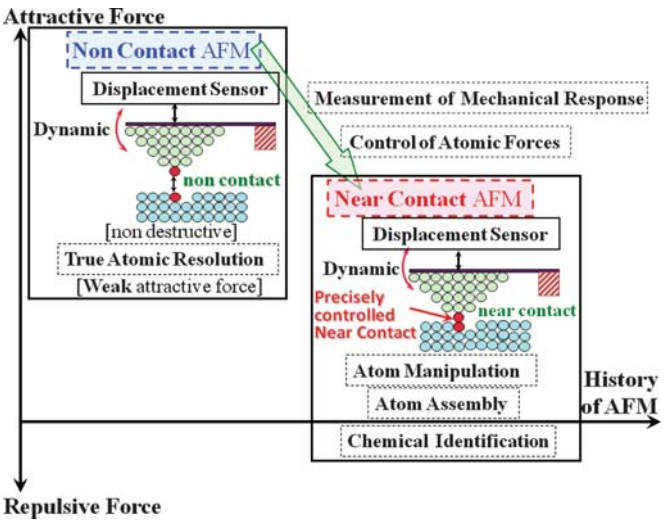

Fig. 1.2. Transition from noncontact AFM (NC-AFM) region for nondestructive topographic imaging to nearcontact (or precisely controlled contact) AFM region for atom manipulation, atom-by-atom assembly, and chemical identification using atomic force spectroscopy

cal manipulation of individual atoms even at RT as introduced in this second volume.

In 2002, we could not build nanostructures by mechanical atom manipulation with AFM. Therefore, atom-by-atom mechanical assembly (true bottom-up nanostructuring) was a dream in AFM field at that time. Now we can construct "Atom Inlay," that is, embedded atom letters, consisting of two atom species even at RT using AFM as introduced in this second volume. Thus, now, all above special features inspired in the previous book are fulfilled by AFM and such rapid development of AFM are completely introduced in this second volume.

1.1.1 Present Status of High Performance AFM

Here we will shortly introduce a few important results in relation with present-day high performance AFM. Those are spatial resolution, chemical coordination effect, and mechanical atom manipulation.

NC-AFM Spatial Resolution Beyond STM

Before 2004, spatial resolution of STM was entirely superior to AFM, because of better signal-to-noise ratio (S/N) of STM with better rigidity and tip–sample distance regulation in conjunction with the tunneling effect. AFM, however, measures chemical bond localized more than moving (spreading) delocalized electron measured by STM. Furthermore, difference of S/N between AFM and STM became smaller recently, so that we achieved AFM spatial resolution better than STM in a few samples [2, 3]. Figure 1.3a–d show successive AFM topographic images of Sn/Si(111)- $(2\sqrt{3} \times 2\sqrt{3})$ surface obtained by decreasing tip–sample distance [3]. Rhombuses indicate the unit cell of $2\sqrt{3} \times 2\sqrt{3}$ surface lattice structure. As unveiled by Fig. 1.4a expanded from Fig. 1.3d and cross-sectional line profile (Fig. 1.4b) obtained along the solid line in Fig. 1.4a [3], by approaching the tip apex toward the sample surface, number of atom observed in the unit cell increases from 4 to 8, because AFM can achieve the highest spatial resolution just before the contact [1]. In case of STM, however, only four atoms were found in the unit cell [4].

Thus, we already achieved AFM spatial resolution beyond STM in a few samples. AFM already demonstrated the possibility to attain even subatomic resolution [5].

Chemical Coordination Effect in NC-AFM Topographic Image

It was found that, in the filled state STM image of (Sn, Pb)/[Si(111), Ge(111)]-$(\sqrt{3} \times \sqrt{3})$ surfaces, relative atom heights of (Sn, Pb) adatoms become higher by increasing the number of the nearest neighbor heterogeneous (Si, Ge) adatoms [6–8]. This is the chemical coordination effect in STM topographic

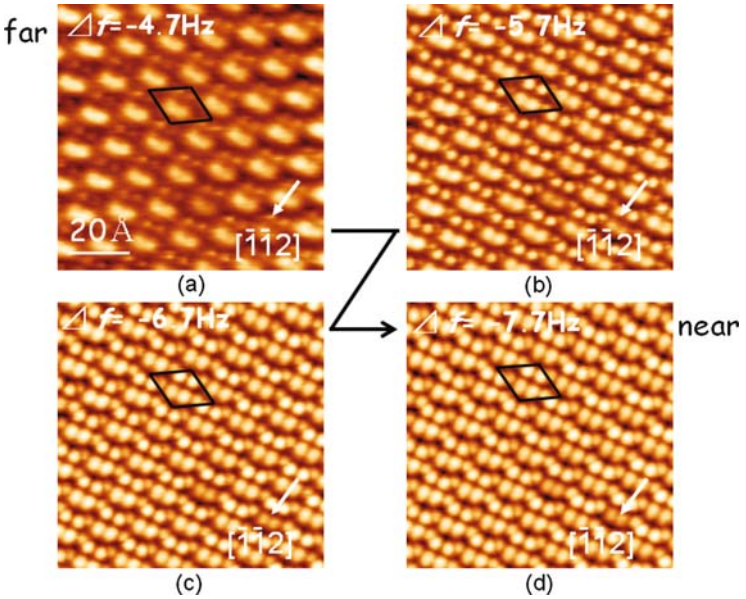

Fig. 1.3. Tip-to-sample distance dependence of NC-AFM topographic image of Sn/Si(111)-$(2\sqrt{3} \times 2\sqrt{3})$ surface from (**a**) far distance to (**d**) near distance, through (**b**) and (**c**) [3]. Rhombuses indicate the unit cell of $2\sqrt{3} \times 2\sqrt{3}$ surface lattice structure. By approaching the tip apex toward the sample surface, number of atom observed in the unit cell increases from 4 to 8

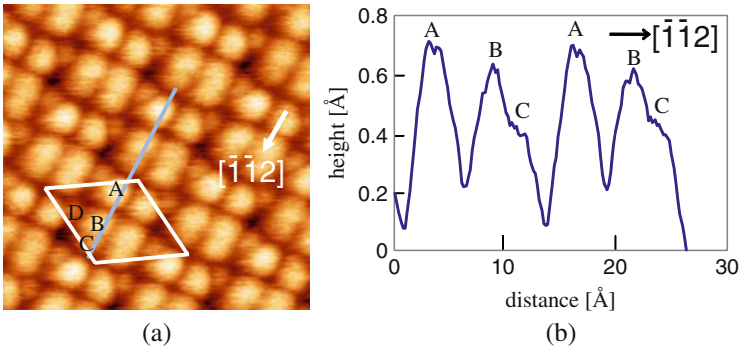

Fig. 1.4. (**a**) NC-AFM image expanded from Fig. 1.3d, and (**b**) cross-sectional line profile obtained along the *solid line* in (**a**) [3]

image. Therefore, its mechanism has been intensely investigated [6–8], and was attributed to the effects induced by electron transfer from (Si, Ge) dangling bond orbital to the nearest neighbor (Sn, Pb) dangling bond orbital. By investigating such coordination effect in NC-AFM topographic images, the imaging mechanism of NC-AFM will be clarified in more detail, but there was

no report in 2002. To measure such chemical coordination effect, NC-AFM with a single pm vertical resolution is crucial.

Experimentally, surrounding atom dependence of relative atom height of Sn adatom (open square) in filled state STM topographic image of Sn/Si(111)-($\sqrt{3}\times\sqrt{3}$) surface [6] is very clear and agrees well with the calculated one (filled square) [7] as shown in Fig. 1.5. On the other hand, theoretical simulation on Pb/Si(111)-($\sqrt{3}\times\sqrt{3}$) surface [8] suggests that the dangling bond of Si adatom has always empty orbital regardless of the coordination number, and that there is no corresponding coordination effect for Si adatom (open circle, filled circle) [6, 7].

In case of NC-AFM topographic image of Sn/Si(111)-($\sqrt{3}\times\sqrt{3}$) surface [9, 10] as well as Pb/Si(111)-($\sqrt{3}\times\sqrt{3}$) surface [10], however, relative atom height of Si adatom (filled triangle) shows clear coordination number dependence as shown in Fig. 1.5. Thus, NC-AFM has different chemical coordination mechanism. Accordingly, by investigating such surrounding atom

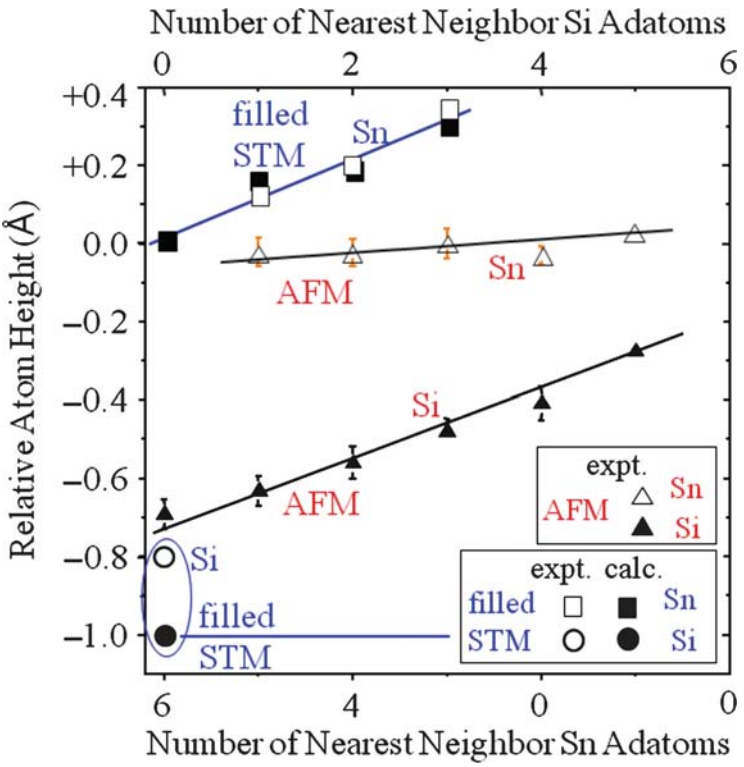

Fig. 1.5. Relative atom height of Si and Sn adatoms in Sn/Si(111)-($\sqrt{3}\times\sqrt{3}$) intermixed surface measured by filled state STM topographic image and NC-AFM topographic image as a function of the chemical coordination number at RT. [expt.] and [calc.] show experimental and theoretically calculated results

dependence of relative atom heights in NC-AFM topographic images, the imaging mechanism of NC-AFM will be clarified in more detail. On the other hand, such chemical coordination effect in intermixed heterogeneous surface will deteriorate chemical discrimination potential of NC-AFM topographic image (so-called atom selective image) using height difference between heterogeneous atoms.

Mechanical Atom Manipulation Under Nearcontact Region

In 2002, by decreasing the tip–sample distance and by varying the noncontact region to the nearcontact region (Fig. 1.2), vertical atom manipulation (removal of Si adatom) by mechanical vertical contact of AFM tip apex with Si(111)7×7 sample surface was tentatively realized at 9.3 K [1]. Immediately, both removal and deposition of Si adatom were successfully demonstrated at 78 K [11]. Then, by precisely controlling the tip–sample distance and by alternately changing the noncontact region and the nearcontact region, site-by-site lateral atom manipulation of single Ge atom adsorbed on Ge(111)-c(2×8) surface was carried out using the raster scan under the nearcontact region at 80 K [12]. Finally, novel atom manipulation phenomena were discovered at RT. Those are lateral and vertical atom interchange manipulations. By using the lateral atom interchange manipulation combined with the vector scan under the nearcontact region, substituted Sn adatoms embedded in Ge(111)-c(2×8) substrate were laterally interchanged 120 times with the selected adjacent Ge adatoms. Then a protruded "Atom Inlay," that is, embedded atom letters consisted of a little large Sn atoms embedded in a little small Ge atoms was constructed at RT as shown in Fig. 1.6a [13]. On the other hand, by using the vertical atom interchange manipulation induced by mechanical vertical contact, tip apex Si atoms were directly interchanged 11 times with the selected Sn adatoms of Sn/Si(111)-$(\sqrt{3} \times \sqrt{3})$ surface. As a result, a hol-

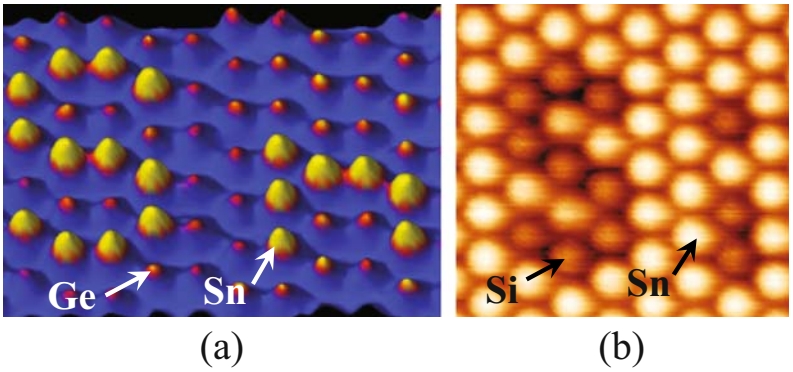

Fig. 1.6. (**a**) A protruded "atom inlay" [13] and (**b**) a hollowed "atom inlay" [14] constructed by atom-by-atom assembly

lowed "Atom Inlay" consisting of a little small Si adatom embedded in a little large Sn adatom was constructed at RT as shown in Fig. 1.6b [14]. The latter is a true single atom pen method using a Si tip apex.

Thus, AFM can construct embedded atom letters consisting of two atom species even at RT. Furthermore, AFM can measure the force needed to move single atom/molecule [15, 16].

1.2 Future Prospects for High Performance AFM

As written in Table 1.1, many topics continuously appeared in annual non-contact AFM conference. Thus, high performance AFM field are still rapidly growing every year. Here, we will briefly introduce several significant regions in relation with future AFM fields.

1.2.1 Atomic and Molecular Imaging in Liquids

In 2002, true atomic resolution was possible only under ultrahigh vacuum (UHV) environment. In air and liquid environments, Q-factor of mechanical resonant oscillation of cantilever drastically reduces and the small Q-factor gets disturbed to obtain atomic resolution. In 2005, by improving frequency noise in frequency modulation (FM) detection method and using small oscillation amplitude of cantilever, vertical and lateral resolutions of 2-6 and 300 pm were achieved, respectively, even with a low Q-factor in water [17]. Such true atomic resolution in water with the minimum deflection noise density of $5.7\,\mathrm{fm}/\sqrt{\mathrm{Hz}}$ in air and $7.3\,\mathrm{fm}/\sqrt{\mathrm{Hz}}$ in water [18] will open the door to atomic scale imaging of biological materials in liquids and atomic scale science taking place at the liquid/solid interface.

1.2.2 Magnetic Exchange Force Microscopy

In the previous book, the short-range magnetic exchange force interaction between a ferromagnetic Fe-coated tip and a NiO(001) surface was explored at RT by using a magnetic tip as a force sensor. As a result, atomically resolved NC-AFM topographic image showed topographic asymmetry of the different directions on oxygen sites, which seems to have a correlation with the spin alignment of NiO(001) surface. This early attempt, however, did not use an external magnetic field to align the magnetic polarization at the tip apex and also low temperature. As a result, topographic asymmetry of the different directions was uncertain and less than a value of about 1%. Besides, they could not observe asymmetry by Fourier transforms of their raw data because of insufficient S/N. Recently, by applying an external magnetic field of $B_{\mathrm{ext}} = 5\,\mathrm{T}$ perpendicular to the sample surface for the magnetic polarization of the iron film of the tip, the topographical asymmetry increased up to about

Table 1.1. Noncontact AFM conferences

Year Date	Location	Papers/ Persons	Topics
1998 July 21–23	Osaka, Japan	47/104	True Atomic Resolution [TiO_2, Ag, Cu, NaCl, TGS, HOPG at LT], Atomically resolved (KPFM, dissipation), Force curve, Theory, Tip-sample dependence of image [Si(111)$\sqrt{3}\times\sqrt{3}$-Ag, InAs at LT], C_{60}
1999 Sept. 1–4	Pontresina, Switzerland	99/134	Alkanethiol, NiO, (Au^-, Al^-)/Si(111)7×7, Higher flexural mode, Submolecule resolution (adenine, thymine), Bias dependence
2000 July 16–19	Hamburg, Germany	93/176	Imaging mechanism [negative or positive tip] of insulators (CaF_2), Cu^-TBPP/Cu(100), $HCOO^-$, CH_3COO^-/TiO_2, (Xe/HOPG, NiO) at LT, Dissipation, Si(111)2×1-Sb
2001 Sept. 2–5	Kyoto, Japan	101/163	($RCOO^-/TiO_2$)[R=H, CH_3, $C(CH_3)_3$, C≡CH, CHF_2, CF_3], qPlus sensor, Alkali halides, CeO_2, Imaging mechanism of molecules
2002 August 11–14	Montreal, Canada	88/121	Vertical atom manipulation, Chemical identification using height difference, KPFM of Si(111)5$\sqrt{3}\times5\sqrt{3}$-Sb, NC-AFM/STM of Cu(100)-c(2×2)N, MgO, Sub-Å oscillation amplitude, BCO SAM, Oxygen adsorbed Si(111)7×7, Vortex
2003 Aug. 31– Sept. 3	Dingle, Ireland	84/111	Subatomic resolution, Theory of Si(111)$\sqrt{3}\times\sqrt{3}$-Ag, Simulated force curves of CaF_2, Submolecule resolution of CuPc, Lateral mode image of Si(111)7×7, (O_2, CH_3OH, NO_2)/CeO_2, Na/TiO_2
2004 Sept. 12–14	Seattle, USA	92/109	Lateral interchange atom manipulation, Embedded atom letters, Lateral atom manipulation, Laser cooling of cantilever, (Atomic image, Force curves) of SWCNT, (Sub Å resolution, CaF_2) with qPlus sensor, Surrounding atom effect on NC-AFM topography, Molecular resolution in air, Scanning nonlinear dielectric microscopy (SNDM)

(*continued*)

Table 1.1. (continued)

2005 August 15–18	Bad Essen, Germany	104/150	Lateral Mnipulation of atomic defects on (CaF_2, KCl) at RT, Lateral manipulation of Si(111)7×7 adatom at RT, Molecular resolution in liquid, Atom tracking for force spectroscopy, H_2O dissociation/TiO_2, O_2 dissociation/CeO_2, SNDM data storage
2006 July 16–20	Kobe, Japan	128/229	Single-atom chemical recognition, Vertical interchange atom manipulation, Si(111)7×7 by SNDM, Magnetic exchange force microscopy, Rapid scan AFM, Potential mapping of Si(111)7×7 at RT, Photoswitching single-molecular tip, Atomic resolution in liquid, Subatomic resolution of tip-atom by CO on Cu(111)
2007 Sept. 16–20	Antalya, Turkey	96/102	Force measurement during atomic manipulation at LT, Tip effect on (TiO_2, MExFM, PTCDA), Alumina oxide on NiAl, Subsurface oxygen vacancy ordering on reduced CeO_2, Force mapping of NaCl, Theory of MExFM, Local solvation force, Laser cooling of cantilever down to 44 mK, (C_{60}, STO, HOPG) with SNDM, Short-range electrostatic force in KPFM
2008 Sept. 16–19	Madrid, Spain	131/180	3D Force and damping maps on nanotube peapods, Theory of vertical interchange atom manipulation, Water chemistry on (CeO_2, CaF_2), Charge state and imaging of a single atom, Si-tip imaging of TiO_2, Vertical and lateral force mapping, MExFM of Fe/W(001), Hydration structures, Atom-manipulation on Cu(111)-O at LT, High- speed AFM in liquid with atomic resolution, Short-range chemical interaction driven zero tunneling current, Superstructure in KBr/(Cu, NaCl)
2009	(New Haven, USA)		
2010	(Kanazawa, Japan)		

17% on the nickel atom sites [19]. Both atomically resolved unfiltered data sets and the Fourier transformed sets for 30 pm difference of tip–sample distance clearly showed the 1×1 at far distance and the (2×1) at near distance, respectively [19]. The (2×1) is antiferromagnetic surface unit cell of NiO(001). Magnetic exchange force microscopy based on AFM can detect the short-range magnetic exchange force interaction between a magnetic tip and a magnetic sample, and observe the arrangement of spins with atomic resolution even on insulating surface. Therefore, such spin imaging based on AFM will contribute to understanding magnetism on the atomic scale.

1.2.3 Rapid Growth of Tuning Fork/qPlus Sensor

AFM based on tuning fork (cf. qPlus sensor) now demonstrated several advantages. It is a kind of self-detection AFM so that it is compatible with conventional STM instrument with atomic resolution. In other words, AFM with atomic resolution can be incorporated with conventional STM instrument with atomic resolution. As a result, it progresses from a simple STM instrument to combined AFM/STM instrument with atomic resolution. Therefore, it can simultaneously observe atomically resolved AFM and STM images and has the potential ability of simultaneous spectroscopy (AFS and STS) [20]. Further, it can use small amplitude less than 10 pm and hence achieve high signal-to-noise ratio (S/N). It can achieve subatomic resolution [5,21]. Besides, it can mechanically manipulate metal atom/molecule [16]. Therefore, we can expect rapid growth of such AFM/STM based on tuning fork (cf. qPlus sensor) that will incorporate STM field with AFM field.

1.2.4 Differentiation of Atomic Force

Atomic force in AFM means chemical force between tip apex atom/molecule and sample surface atom/molecule. Besides chemical force between interacting atoms/molecules includes various kinds of force such as covalent bonding force, ionic bonding force, metallic bonding force, van der Waals force, and hydrogen bonding force. Therefore, by investigating the imaging mechanism of AFM with various samples and tips in more detail, differentiation of atomic force will progress at the atomic scale. In case of ionic crystals such as $CaF_2(111)$ surface, we already know that short-range electrostatic force is the origin of atomically resolved image. In this case, tip will pick up small cluster of ionic crystal, and then picked-up tip works as positive or negative tip depending on topmost ion species with positive or negative charge. As a result, because of the attractive force imaging method in noncontact AFM, positive tip can image only negative surface ion (anion), while negative tip can image only positive surface ion (cation) [22]. In case of $TiO_2(110)$ surface, however, quite seldom Si tip that can form covalent-like bond and hence image the real topographic structure of the surface was found in addition to positive and negative tip [23]. In case of molecular samples, van der Waals force and

polarization force contribute to AFM imaging [1]. Thus, by investigating the imaging mechanism of AFM with various samples and tips in more detail, difference of imaging mechanism will become clearer and hence differentiation of atomic force in AFM will progress at the atomic scale. Besides, such investigation will disclose the bonding nature between various atom pairs in more detail.

1.2.5 Atom-by-Atom Assembly of Complex Nanostructure at RT

The nanostructure is the base of the quantum effect. On the other hand, multi atom species are a key issue for functional materials. Therefore, complex nanostructures consisting of multiatom species will combine the quantum effect with functional materials and hence deliver abundant novel functional materials/devices. To construct complex nanostructures, true bottom-up nanostructuring, that is, atom-by-atom assembly, is crucial. It requires, first, imaging and chemical identification of individual atoms [9, 10, 24] (Fig. 1.7a), second, atom manipulation of selected atom species to the designed site [11, 12, 15] (Fig. 1.7b), and finally, atom-by-atom assembly of complex nanostructures [13, 14] (Fig. 1.7c).

Recently, these three procedures were developed based on AFM. As a result, a kind of complex nanostructures consisting of two atom species, protruded "Atom Inlay" [13] (Fig. 1.6a) and a hollowed "Atom Inlay" [14] (Fig. 1.6b), were constructed at RT. Now we can try to construct complex atom clusters/wires consisting of multiatom species. Such research will disclose the bonding nature and chemical coordination effect of various atom species consisting complex nanostructures in more detail. In future, we may investigate the possibility to construct more complex nanostructures such as molecule and polymer.

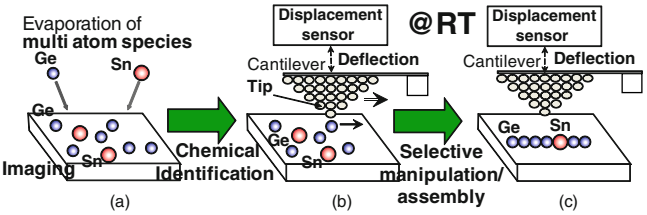

Fig. 1.7. Atom-by-atom assembly of complex nanostructure at RT. (**a**) Imaging and chemical identification of individual atoms, (**b**) atom manipulation of selected atom species to the designed site, and (**c**) atom-by-atom assembly of complex nanostructures

References

1. S. Morita, R. Wiesendanger, E. Meyer, *Noncontact Atomic Force Microscopy* (Springer, Berlin, 2002)
2. T. Eguchi, Y. Fujikawa, K. Akiyama, T. An, M. Ono, T. Hashimoto, Y. Morikawa, K. Terakura, T. Sakurai, M.G. Lagally, Y. Hasegawa, Phys. Rev. Lett. **93**, 266102 (2004)
3. Y. Sugimoto, M. Abe, S. Hirayama, S. Morita, Nanotechnology **17**, 4235 (2006)
4. L. Ottaviano, G. Profeta, L. Petaccia, C.B. Nacci, S. Santucci, Surf. Sci. **554**, 109 (2004)
5. F.J. Giessibl, S. Hembacher, H. Bielefeldt, J. Mannhart, Science **289**, 422 (2000)
6. S.T. Jemander, N. Lin, H.M. Zhang, R.I.G. Uhrberg, G.V. Hansson, Surf. Sci. **475**, 181 (2001)
7. W. Kaminski, P. Jelinek, R. Perez, F. Flores, J. Ortega, Appl. Surf. Sci. **234**, 286 (2004)
8. M. Švec, P. Jelinek, P. Shukrynau, C. Gonzalez, V. Chab, Phys. Rev. B **77**, 125104 (2008)
9. Y. Sugimoto, M. Abe, K. Yoshimoto, O. Custance, I. Yi, S. Morita, Appl. Surf. Sci. **241**, 23 (2005)
10. A. Ohiso, M. Hiragaki, K. Mizuta, Y. Sugimoto, M. Abe, S. Morita, e-J. Surf. Sci. Nanotechnol. **26**, 79 (2008)
11. N. Oyabu, O. Custance, I. Yi, Y. Sugawara, S. Morita, Phys. Rev. Lett. **90**, 176102 (2003)
12. N. Oyabu, Y. Sugimoto, M. Abe, O. Custance, S. Morita, Nanotechnology **16**, S112 (2005)
13. Y. Sugimoto, M. Abe, S. Hirayama, N. Oyabu, O. Custance, S. Morita, Nat. Mater. **4**, 156 (2005)
14. Y. Sugimoto, P. Pou, O. Custance, P. Jelinek, M. Abe, R. Perez, S. Morita, Science **322**, 413 (2008)
15. Y. Sugimoto, P. Jelinek, P. Pou, M. Abe, S. Morita, R. Perez, O. Custance, Phys. Rev. Lett. **98**, 106104 (2007) and its additional information
16. M. Ternes, C.P. Lutz, C.F. Hirjibehedin, F.J. Giessibl, A.J. Heinrich, Science **319**, 1066 (2008)
17. T. Fukuma, K. Kobayashi, K. Matsushige, H. Yamada, Appl. Phys. Lett. **86**, 193108 (2005)
18. T. Fukuma, S.P. Jarvis, Rev. Sci. Instrum. **77**, 043701 (2006)
19. U. Kaiser1, A. Schwarz, R. Wiesendanger, Nature **446**, 522 (2007)
20. M. Herz, C. Schiller, F.J. Giessibl, J. Mannhart, Appl. Phys. Lett. **86**, 153101 (2005)
21. S. Hembacher, F.J. Giessibl, J. Mannhart, Science **305**, 380 (2004)
22. C. Barth, A.S. Foster, M. Reichling, A.L. Shluger, J. Phys. Condens. Matter. **13**, 2061 (2001)
23. G.H. Enevoldsen, A.S. Foster, M.C. Christensen, J.V. Lauritsen, F. Besenbacher, Phys. Rev. B **76**, 205415 (2007)
24. Y. Sugimoto, P. Pou, M. Abe, P. Jelinek, R. Perez, S. Morita, O. Custance, Nature **446**, 64 (2007)